REGULAR ARTICLE

# Theoretical study of one- and two-photon absorption properties of pyrene derivatives

Yang Zhao · Jing-Fu Guo · Ai-Min Ren ·
Ji-Kang Feng

**Abstract** The geometrical structure, electronic structure, one-photon absorption (OPA) properties of pyrene and its derivatives have been theoretically studied by using density functional theory (DFT) method and Zerner's intermediate neglect of differential overlap (ZINDO) methods, and their two-photon absorption (TPA) properties are calculated by the ZINDO/sum-over-states method. The results show that introducing donor groups to pyrene molecule, increasing the number of donor groups, extending the conjugated length, or forming circular conjugated dimer can increase the oscillator strength ($f$) in the TPA process and ultimately result in extremely large TPA cross-sections and strong OPA around 400 nm of pyrene derivatives. All these results give us some basic principles to design pyrene derivatives with large TPA cross-sections. This shed light into the significance of the pyrene derivatives as promising fluorescent probes in biochemistry when they were linked to some special recognizing groups.

**Keywords** Pyrene derivatives · One-photon absorption · Two-photon absorption · Two-photon absorption cross-section · Electronic structure

Y. Zhao · A.-M. Ren (✉) · J.-K. Feng
State Key Laboratory of Theoretical and Computational
Chemistry, Institute of Theoretical Chemistry,
Jilin University, 130023 Changchun,
People's Republic of China
e-mail: aimin_ren@yahoo.com

J.-F. Guo
School of Physics,
Northeast Normal University,
130021 Changchun,
People's Republic of China

## 1 Introduction

Since two-photon absorption (TPA) phenomenon was first predicted by Maria Göppert-Mayer in 1931 [1], interest in TPA materials has increased over the past decade year. Up to now, materials with large TPA cross-section have been utilized for a myriad of optical applications such as three-dimensional (3D) optical storage memory [2, 3], two photon microscopy [4, 5], upconverted lasing [6], optical power limiting [7], photodynamic therapy [8] and two photon fluorescence probe [9]. As a third-order nonlinear optical process, TPA was induced by simultaneous absorption of two photons of identical and different frequencies in order to excite a molecule from the ground state to a higher energy electronic state. Comparing with linear absorption (one-photon absorption), higher penetrating depth and lower scattering light are feasible in TPA system. The major advantage of TPA activity is that the absorption light strength of a TPA process dependent on the square of the irradiance, which makes it possible to confine the laser excitation in a minute spatial volume and drops off sharply on all side. But until now, the practical TPA materials are still limited, explore and research new materials with potential TPA properties is urgent.

As an excellent TPA material, one of the most important features is that it must exhibit large TPA cross-section. In a previous study, we have investigated the TPA properties of perylene tetracarboxylic derivatives [10]. Results showed that the molecular $\pi$-center with good rigidity will bring on a large TPA cross-section and be benefit for TPA applications. Herein we designed and investigated a series of compounds based on pyrene molecule with good rigidity. It is reported that pyrene as an attractive $\pi$–conjugated group are one of the most useful fluorogenic unit and it has been applied in various areas over recent years. For example

organic semiconductor, liquid crystal, organic light-emitting diodes and photoactive polypeptides [11–14]. Especially pyrene can be used as various of microenvironment probe when it was linked to some special structure as a fluorescent substituent [15–19]. Generally, these probes have excellent properties such as with high sensitivity, good selectivity, and among them, the most important one is that most of the pyrene derivatives have quite high fluorescent quantum yields (Φ) due to its large two-photon absorption cross-section and this makes them widely used in biochemistry, such as detection of target DNAs, DNA hybridization detection, DNA mismatch detection, and probing DNA sequences, etc. [17, 20–26]. In 2008, Kim et al. first reported on the utilizing of pyrene as a TPA material. They synthesized a series of pyrene derivatives with 4-(N, N-dimethylamino) phenylethynyl group as substituent [27]. Their investigation reveals that pyrene is an efficient π-center in two photon materials, and its derivatives provide large TPA cross-sections (δ) and present high Φ nearly to 1.0 which can compare with the most efficient two photon materials. The δ values of these compounds increase with the number of substituent, but the intrinsic origin is still unclear. To the best of our knowledge, systemic theoretical study on TPA properties of pyrene derivatives has not been reported to date. So the design and detailed investigation on more efficient TPA materials bearing pyrene as a π-center is necessary and urgent. Herein, we designed a series of pyrene derivatives and theoretically studied the intrinsic relations between molecular structure and one- and two-photon properties, including (1) molecular structure design and electronic structure characterize: optimized geometries show that the planar rigid molecular backbone and extended π-conjugate provide a possibility of this kind of molecules bearing large TPA cross-sections, (2) the electronic spectra profile: monotonic-increasing conjugated length is an effective measures of Uv–vis spectrum red-shift. Forming circular conjugated dimer make the Uv–vis spectrum change slightly, but the oscillator strengths are effectively enlarged, (3) the TPA property origin: this part reveals that the transition dipole moment, excitation energy and the oscillator strength (f) in the TPA process are all the intrinsic origins of the enlargement of TPA cross-section.

## 2 Computational method

The TPA process corresponds to simultaneous absorption of two photons. The TPA efficiency of an organic molecule, at optical frequency $\omega/2\pi$, can be characterized by the TPA cross-section $\delta(\omega)$. It can be directly related to the imaginary part of the second hyperpolarizability $\gamma(-\omega; \omega, -\omega, \omega)$ [28, 29], as shown in Eq. 1:

$$\delta(\omega) = \frac{3\hbar\omega^2}{2n^2c^2\varepsilon_0}L^4 \mathrm{Im}[\gamma(-\omega; \omega, -\omega, \omega)] \tag{1}$$

where $\gamma(-\omega; \omega, -\omega, \omega)$ is the third-order molecular polarizability, $\hbar\omega$ the energy of the incoming photons, $c$ is the speed of light, $\varepsilon_0$ is the vacuum electric permittivity, $n$ denotes the refractive index of the medium and $L$ corresponds to the local-field factor. In the calculations presented here, $n$ and $L$ are set to 1 because the isolated molecule is in the vacuum.

The sum-over-states (SOS) expression to evaluate the components of the second hyperpolarizability $\gamma(-\omega; \omega, -\omega, \omega)$ can be educed using perturbation theory. By considering a Taylor expansion of the energy with respect to the applied field, the Cartesian components of $\gamma$ are given by [30, 31]:

$$\gamma_{\alpha\beta\gamma\delta}(-\omega_\sigma; \omega_1, \omega_2, \omega_3) = \hbar^{-3}\sum P_{1,2,3}$$

$$\left(\sum_K{}'\sum_L{}'\sum_M{}'\left(\frac{\langle 0|\mu_\alpha|K\rangle\langle K|\overline{\mu_\beta}|L\rangle\langle L|\overline{\mu_\gamma}|M\rangle\langle M|\mu_\delta|0\rangle}{(\omega_K - i\Gamma_K - \omega_\sigma)(\omega_L - i\Gamma_L - \omega_2 - \omega_3)(\omega_M - i\Gamma_M - \omega_3)}\right.\right.$$

$$+\frac{\langle 0|\mu_\beta|K\rangle\langle K|\overline{\mu_\alpha}|L\rangle\langle L|\overline{\mu_\gamma}|M\rangle\langle M|\mu_\delta|0\rangle}{(\omega_K + i\Gamma_K + \omega_1)(\omega_L - i\Gamma_L - \omega_2 - \omega_3)(\omega_M - i\Gamma_M - \omega_3)}$$

$$+\frac{\langle 0|\mu_\beta|K\rangle\langle K|\overline{\mu_\gamma}|L\rangle\langle L|\overline{\mu_\alpha}|M\rangle\langle M|\mu_\delta|0\rangle}{(\omega_K + i\Gamma_K + \omega_1)(\omega_L + i\Gamma_L + \omega_1 + \omega_2)(\omega_M - i\Gamma_M - \omega_3)}$$

$$\left.+\frac{\langle 0|\mu_\beta|K\rangle\langle K|\overline{\mu_\gamma}|L\rangle\langle L|\overline{\mu_\delta}|M\rangle\langle M|\mu_\alpha|0\rangle}{(\omega_K + i\Gamma_K + \omega_1)(\omega_L + i\Gamma_L + \omega_2 + \omega_3)(\omega_M + i\Gamma_M + \omega_\sigma)}\right)$$

$$-\sum_K{}'\sum_L{}'\left(\frac{\langle 0|\mu_\alpha|K\rangle\langle K|\mu_\beta|0\rangle\langle 0|\mu_\gamma|L\rangle\langle L|\mu_\delta|0\rangle}{(\omega_K - i\Gamma_K - \omega_\delta)(\omega_K - i\Gamma_K - \omega_1)(\omega_L - i\Gamma_L - \omega_3)}\right.$$

$$+\frac{\langle 0|\mu_\alpha|K\rangle\langle K|\mu_\beta|0\rangle\langle 0|\mu_\gamma|L\rangle\langle L|\mu_\delta|0\rangle}{(\omega_K - i\Gamma_K - \omega_1)(\omega_L + i\Gamma_L + \omega_2)(\omega_L - i\Gamma_L - \omega_3)}$$

$$+\frac{\langle 0|\mu_\beta|K\rangle\langle K|\mu_\alpha|0\rangle\langle 0|\mu_\gamma|L\rangle\langle L|\mu_\delta|0\rangle}{(\omega_K + i\Gamma_K + \omega_1)(\omega_K + i\Gamma_K + \omega_\delta)(\omega_L + i\Gamma_L + \omega_2)}$$

$$\left.\left.+\frac{\langle 0|\mu_\beta|K\rangle\langle K|\mu_\alpha|0\rangle\langle 0|\mu_\gamma|L\rangle\langle L|\mu_\delta|0\rangle}{(\omega_K + i\Gamma_K + \omega_1)(\omega_L + i\Gamma_L + \omega_2)(\omega_L - i\Gamma_L - \omega_3)}\right)\right) \tag{2}$$

In this formula $\alpha$, $\beta$, $\gamma$ and $\delta$ refer to the molecular axes; $\omega_1$, $\omega_2$, and $\omega_3$ are optical frequencies and $\omega_\delta = \omega_1 + \omega_2 + \omega_3$ is the polarization response frequency; $\sum P_{1,2,3}$ indicates a sum over the terms obtained by the six permutations of the pairs $(\omega_1/\mu_\beta)$, $(\omega_2/\mu_\gamma)$ and $(\omega_3/\mu_\delta)$; $|K\rangle$ is an electronic wavefunction with energy $\hbar\omega_K$ relative to the ground electronic state; $\mu_\alpha$ is the $\alpha$th ($=x, y, z$) component of the dipole operator, $\langle K|\overline{\mu_\alpha}|L\rangle = \langle K|\mu_\alpha|L\rangle - \langle 0|\mu_\alpha|0\rangle$; the primes on the summation over the electronic states indicate exclusion of the ground state. $\Gamma_K$ is the damping factor of excited state $K$, in the present work, all damping factors $\Gamma_K$ are set to 0.14 eV; this choice of damping factor is found to be reasonable on the basis of the comparison between the theoretically calculated and experimental TPA spectra [32].

To compare the calculated $\delta$ value with the experimental value, the orientationally averaged (isotropic) value of $\gamma$ is evaluated, which is defined as

$$\langle \gamma \rangle = \frac{1}{15} \sum_{i,j} \left( \gamma_{iijj} + \gamma_{ijij} + \gamma_{ijji} \right) \quad i,j = x, y, z \tag{3}$$

where after $\langle \gamma \rangle$ is taken into Eq. 1, and then the TPA cross section $\delta$ is obtained.

$$\delta \propto \frac{M_{0k}^2 M_{kn}^2}{(E_{0k} - E_{0n}/2)^2 \Gamma} + \frac{M_{0n}^2 \Delta \mu_{0n}^2}{(E_{0n}/2)^2 \Gamma} \tag{4}$$

where $M_{ij}$ is the transition dipole moment from the state $i$ to $j$; $E_{ij}$ is the corresponding excitation energy, the subscripts 0, $k$ and $n$ refer to the ground state $S_0$, the intermediate state $S_k$, and the TPA final state $S_n$, respectively; $\Delta \mu_{0n}$ is the dipole moment difference between $S_0$ and $S_n$.

In principle, any kind of self-consistent field molecular orbital theory combined with configuration interaction can be used to calculate the physical values in the above expression. In this paper, the Becke's three-parameter exchange functional in combination with the LYP correlation functional (B3LYP) and the standard 6-31G* basis set were used to calculate molecular equilibrium geometry [33, 34]. Then, UV–Vis spectrum was obtained by single and double electron excitation configuration interaction employing ZINDO method [35]. And the calculated transition dipole moment and the corresponding transition energy can be used to predict the TPA properties. Then, by comibiled program FTR-NLO using Eqs. 1–4, we calculated the second hyperpolarizability $\gamma$ and TPA cross-section $\delta$.

## 3 Results and discussion

### 3.1 Geometry optimization and electron structure

Usually, the important features of molecules with strong TPA are that endowed with a long extended conjugating length and substituted by strong donor or acceptor group which can increase the potential for charge transfer [36–38]. Based on the compounds reported in Kim's work [27], we design a series of pyrene derivatives which is shown in Fig. 1. Using pyrene molecule as a $\pi$-center to keep molecular planarity and rigidity, the 4-(N, N-dimethyl-amino) phenylethynyl group was introduced as a donor substituent to extend the conjugation length. First, molecules P1–P4 were designed by changing the position or increasing the number of donor groups. The two monomer backbones S1 and S2 were built by introducing a different donor group on the basis of P and P2, and T1 and T2 are their corresponding dimers. Molecule Q was designed by replacing the substituent R of molecule T2 with R1 to enhance the donor group strength.

DFT calculations were carried out as implemented in the Gaussian 03 package of quantum chemical programs [39]. And geometry optimizations of all the pyrene molecules were completed by using the DFT/B3LYP/6-31G*. Results showed that all the optimized geometries of pyrene derivatives keep good planarity.

The energies of some frontier orbitals and the energy gaps between the highest occupied molecular orbital



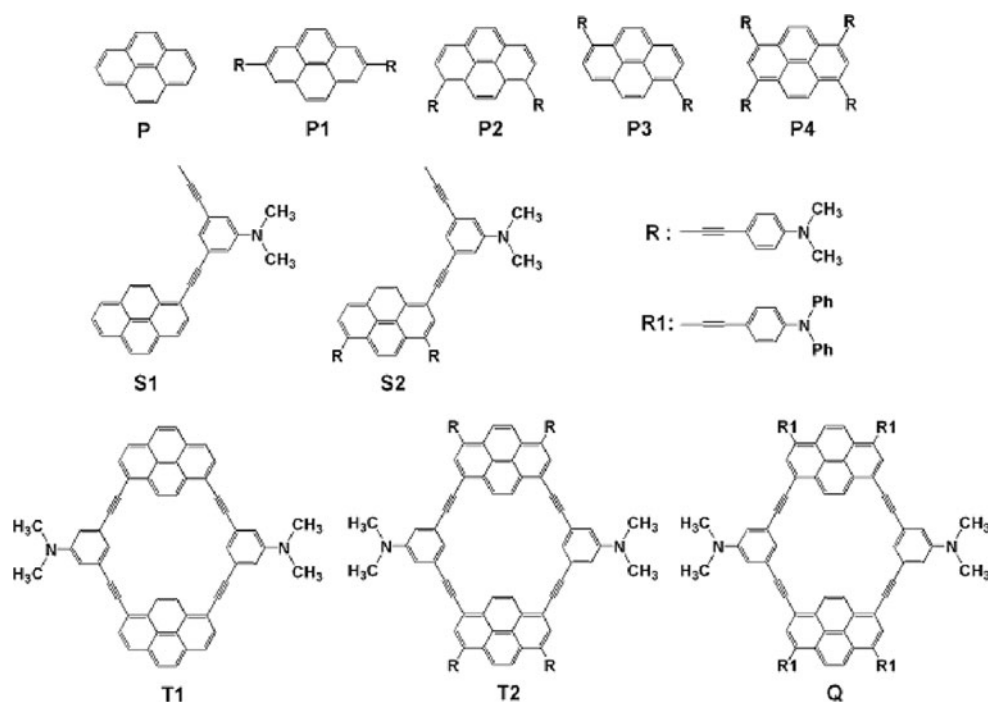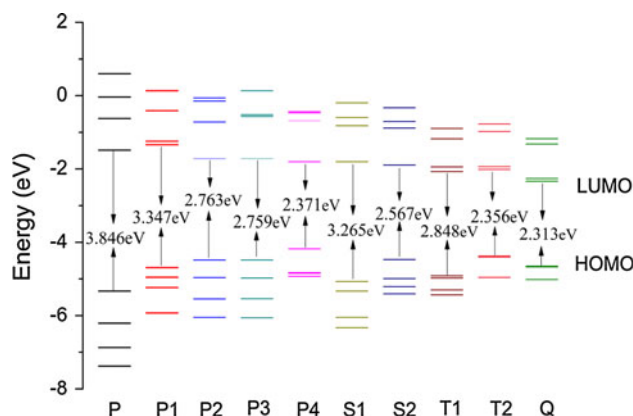**Fig. 1** Molecular structure of pyrene derivatives

**Table 1** The energy of the highest occupied orbital ($E_{HOMO}$) and the energy of the lowest unoccupied orbital ($E_{LUMO}$)

| Energy | P | P1 | P2 | P3 | P4 | S1 | S2 | T1 | T2 | Q |
|---|---|---|---|---|---|---|---|---|---|---|
| $E_{HOMO}$(eV) | −5.3264 | −4.6796 | −4.4747 | −4.4730 | −4.1764 | −5.0695 | −4.4619 | −4.9182 | −4.3696 | −4.6409 |
| $E_{LUMO}$(eV) | −1.4800 | −1.3328 | −1.7119 | −1.7138 | −1.8050 | −1.8050 | −1.8947 | −2.0700 | −2.0134 | −2.3277 |

(HOMO) and the lowest unoccupied molecular orbital
(LUMO) obtained by B3LYP/6-31G* method are listed in
Table 1. For molecule P and its derivatives (P1–P4), as the
number of introducing donor group increased, the energy
of HOMO also increased. And molecule P4 with four
introduced donor groups has the highest energy of HOMO.
Compared with P1, we found that by introducing donor
groups on shoulder position, P2 and P3 have a higher
HOMO energy and a lower energy gap between HOMO
and LUMO ($\Delta E_{H-L}$). So, we selected P and P2 as the
backbone to construct S1 and S2, and the calculated results
also showed the same phenomenon that S1 and S2 have
higher HOMO energy and lower $\Delta E_{H-L}$ than P and P2 by
introducing more donor groups on shoulder position. For
the dimer molecule T1 and T2, they showed the same
energy trend as the molecule S1 and S2. From Table 1 we
can also found that the dimer molecules T1 and T2 have a
higher HOMO energy and a lower LUMO energy than the
monomer molecules S1 and S2. This may be attributed to
the formation of circular dimers, which extended the
conjugation length, and resulted in smaller energy gaps.
This phenomena was clearly shown in Fig. 2, that the
$\Delta E_{H-L}$ decreases with the extension of the conjugated
length (3.846 eV (P) > 3.347 eV (P1) > 2.763 eV (P2) >
2.759 eV (P3) > 2.371 eV (P4), 3.846 eV (P) > 3.265 eV
(S1), 2.763 eV (P2) > 2.567 eV (S2), 3.265 eV (S1) >
2.848 eV (T1), 2.567 eV (S2) > 2.356 eV (T2)).

### 3.2 One-photon absorption (OPA) properties

In view of the close relation with TPA properties, the OPA
properties of the pyrene molecules have been calculated by
employing the ZINDO program, on the basis of the equi-
librium geometries calculated by DFT/B3LYP/6-31G*
method. The calculated OPA wavelengths ($\lambda^{(1)}$), the cor-
responding oscillator strength ($f$) and the transition nature
of the molecules under investigation are listed in Table 2
and some experimental data are given in parentheses. As
shown in Table 2, $\lambda_{max}^{(1)}$ of P2, P3 and P4 (the experimental
values of $\lambda_{max}^{(1)}$ in toluene solvent have already been
reported [27]) were also calculated by employing TDDFT
B3LYP/6-31G* method. Compared the results obtained by
TDDFT and ZINDO method with the experimental results,
the $\lambda_{max}^{(1)}$ calculated by ZINDO method (Table 2) are in
better agreement with the experimental data than that by



**Fig. 2** Molecular orbital diagrams summarizing results predicted by
the B3LYP/6-31G* method

TDDFT method. So, the OPA and TPA properties of all the
pyrene molecules in the following discussions are pre-
dicted by employing ZINDO program.

According to Table 2, molecule P shows only one OPA
peak ($\lambda_{max}^{(1)}$) at 317.1 nm, while its derivatives P1–P4 appear
two OPA peaks, and the $\lambda^{(1)}$ values of these two peaks are all
red shifted relative to molecule P. Among them, the higher
energy absorption bands are all located in the ultraviolet
region, no more than 380 nm, while the lower energy
absorption bands are red shifted to the visible light region
gradually. From Table 2, we can also find that as the number
of the donor groups increased, molecule P4 shows a longer
OPA wavelength than P1, P2 and P3 for its extended con-
jugation length. By introducing new donor groups, the $\lambda_{max}^{(1)}$ of
the two monomer molecules S1 and S2 show an apparent red
shift compared with their framework molecules P and P2, but
they change a little compared with their corresponding dimer
molecules T1 and T2. The main difference between them is
that the dimers have much larger oscillator strength ($f$) than
the monomers. The oscillator strength ($f$) of the dimer
molecule T1 is 1.67721, which is more than two times larger
than the monomer molecule S1. For the dimer molecule T2,
more than two-fold enhancement of OPA intensity is
observed compared with the monomer molecule S2. All these
results showed that the oscillator strength can be effectively
enlarged by adding more conjugated segments or forming
circular conjugation molecule. This was also demonstrated by
molecule Q, which with long conjugation length and strong
donor group shows much larger oscillator strength. As we
know that the $\lambda^{(1)}$ of all the molecules are mainly contributed

**Table 2** OPA properties of pyrene derivatives

| Compound | $\lambda_{max}^{(1)}$/nm | $f$ | Transition nature | |
|---|---|---|---|---|
| P | 317.1 | 0.28071 | $S_0 \rightarrow S_2$ | HOMO $\rightarrow$ LUMO 85% |
| | | | | HOMO-1 $\rightarrow$ LUMO+1 11% |
| P1 | 367.2 | 1.67212 | $S_0 \rightarrow S_2$ | HOMO-2 $\rightarrow$ LUMO+2 15% |
| | | | | HOMO $\rightarrow$ LUMO+1 67% |
| | 339.7 | 0.97180 | $S_0 \rightarrow S_3$ | HOMO-1 $\rightarrow$ LUMO 79% |
| P2 | 442.6 (489.0$^{TDDFT}$, 430$^{exp}$) | 0.95997 | $S_0 \rightarrow S_1$ | HOMO $\rightarrow$ LUMO 84% |
| | 365.0 | 0.94972 | $S_0 \rightarrow S_3$ | HOMO-1 $\rightarrow$ LUMO 44% |
| | | | | HOMO $\rightarrow$ LUMO+1 22% |
| P3 | 437.5 (487.1$^{TDDFT}$, 431$^{exp}$) | 1.46752 | $S_0 \rightarrow S_1$ | HOMO $\rightarrow$ LUMO 84% |
| | 319.9 | 0.57938 | $S_0 \rightarrow S_{10}$ | HOMO-2 $\rightarrow$ LUMO 16% |
| | | | | HOMO-1 $\rightarrow$ LUMO+2 22% |
| | | | | HOMO $\rightarrow$ LUMO+3 18% |
| P4 | 494.0 (565.37$^{TDDFT}$, 508$^{exp}$) | 1.33090 | $S_0 \rightarrow S_1$ | HOMO $\rightarrow$ LUMO 89% |
| | 375.5 | 2.33403 | $S_0 \rightarrow S_4$ | HOMO-1 $\rightarrow$ LUMO 43% |
| | | | | HOMO $\rightarrow$ LUMO+1 25% |
| S1 | 389.0 | 0.77539 | $S_0 \rightarrow S_3$ | HOMO $\rightarrow$ LUMO 75% |
| S2 | 462.3 | 1.20972 | $S_0 \rightarrow S_1$ | HOMO $\rightarrow$ LUMO 87% |
| | 365.3 | 1.12528 | $S_0 \rightarrow S_4$ | HOMO-2 $\rightarrow$ LUMO 21% |
| | | | | HOMO-1 $\rightarrow$ LUMO 10% |
| | | | | HOMO $\rightarrow$ LUMO+1 16% |
| T1 | 402.8 | 1.67721 | $S_0 \rightarrow S_4$ | HOMO $\rightarrow$ LUMO 53% |
| | | | | HOMO-1 $\rightarrow$ LUMO+1 38% |
| T2 | 461.6 | 2.48988 | $S_0 \rightarrow S_2$ | HOMO $\rightarrow$ LUMO 48% |
| | | | | HOMO-1 $\rightarrow$ LUMO+1 44% |
| | 356.5 | 0.64499 | $S_0 \rightarrow S_5$ | HOMO-1 $\rightarrow$ LUMO+4 14% |
| | | | | HOMO $\rightarrow$ LUMO+6 17% |
| | 348.5 | 5.93928 | $S_0 \rightarrow S_8$ | HOMO-3 $\rightarrow$ LUMO 13% |
| | | | | HOMO-2 $\rightarrow$ LUMO+1 14% |
| | | | | HOMO $\rightarrow$ LUMO+3 14% |
| Q | 461.6 | 2.66419 | $S_0 \rightarrow S_2$ | HOMO-1 $\rightarrow$ LUMO 46% |
| | | | | HOMO $\rightarrow$ LUMO+1 45% |
| | 353.9 | 6.16283 | $S_0 \rightarrow S_5$ | HOMO-3 $\rightarrow$ LUMO 14% |
| | | | | HOMO-2 $\rightarrow$ LUMO+1 14% |
| | | | | HOMO-1 $\rightarrow$ LUMO+2 12% |
| | | | | HOMO $\rightarrow$ LUMO+3 11% |

by some lower energy excitations of the important excited states, such as HOMO to LUMO, HOMO-1 to LUMO, and HOMO to LUMO+1. The $\lambda^{(1)}$ in lower energy absorption bands are mainly characterized as HOMO $\rightarrow$ LUMO transition. This is just corresponding to the trend of $\Delta E_{H-L}$.

In addition, the calculated $\lambda^{(1)}$ values of most of the molecules studied located around 400 nm, which indicated that these pyrene derivatives retained a good transparency.

### 3.3 Two-photon absorption (TPA) properties

Based on correct OPA spectra, TPA properties are calculated by the ZINDO and FTRNLO programs. The calculated TPA maximal absorption wavelength ($\lambda_{max}^{(2)}$), imaginary part of the second hyperpolarizability (Im$\gamma$), the maximal TPA cross-section ($\delta_{max}$), and the transition channel are all listed in Table 3. The TPA values related to the experimental wavelengths are listed too. The TPA spectra in the incident wavelength are also constructed in Fig. 3 to provide a clearer comparison between the molecules studied. Almost all the pyrene derivatives studied in this work present two TPA peaks except P4, and the $\delta$ values in the shorter wavelength band are larger than that in the longer wavelength band. For molecule P1, P2, and P3, as the substituents introduced, the $\delta$ values are all increased; furthermore, the $\delta$ values in the shorter and longer wavelength band for each molecule are

**Table 3** TPA properties of pyrene derivatives

| Compound | $\lambda_{max}^{(2)}$/nm | Im$\gamma$/1 × 10$^{-34}$ esu | $\delta$/(10$^{-50}$ cm$^4$ s photon$^{-1}$) | Transition nature | |
|---|---|---|---|---|---|
| P | 407.04 | 3,373 | 335.81 | $S_0 \to S_{17}$ | HOMO-3 → LUMO 21% |
| | | | | | HOMO-2, HOMO → LUMO, LUMO+2 12% |
| | | | | | HOMO, HOMO → LUMO, LUMO 21% |
| | 341.18 | 5,420 | 768.03 | $S_0 \to S_{40}$ | HOMO-1 → LUMO+8 21% |
| P1 | 548.61 | 20,834 | 1,141.77 | $S_0 \to S_{17}$ | HOMO-2 → LUMO+1 17% |
| | | | | | HOMO → LUMO+6 27% |
| | 423.74 | 28,556 | 2,623.31 | $S_0 \to S_{42}$ | HOMO-3 → LUMO+2 12% |
| | | | | | HOMO-2, HOMO-1 → LUMO, LUMO+2 13% |
| | | | | | HOMO-1, HOMO → LUMO, LUMO+1 20% |
| P2 | 568.22 (760$^{exp}$, 713$^{ZINDO}$) | 33,411 | 1,706.86 (230$^{exp}$, 165$^{ZINDO}$) | $S_0 \to S_{16}$ | HOMO-3 → LUMO 39% |
| | | | | | HOMO → LUMO+1 12% |
| | | | | | HOMO → LUMO+7 23% |
| | 476.50 | 112,868 | 8,199.46 | $S_0 \to S_{30}$ | HOMO-1 → LUMO+3 16% |
| | | | | | HOMO → LUMO+8 15% |
| | | | | | HOMO, HOMO → LUMO, LUMO 15% |
| P3 | 522.26 (760$^{exp}$, 731$^{ZINDO}$) | 77729 | 4700.53 (490$^{exp}$, 347$^{ZINDO}$) | $S_0 \to S_{20}$ | HOMO-4 → LUMO 16% |
| | 476.50 | 156,221 | 11,348.87 | $S_0 \to S_{30}$ | HOMO → LUMO+8 11% |
| | | | | | HOMO-1, HOMO → LUMO, LUMO+2 10% |
| | | | | | HOMO, HOMO → LUMO, LUMO 31% |
| P4 | 541.42 (820$^{exp}$, 736$^{ZINDO}$) | 345,834 | 19,459.78 (1,150$^{exp}$, 557$^{ZINDO}$) | $S_0 \to S_{31}$ | HOMO-2 → LUMO+1 24% |
| | | | | | HOMO → LUMO+2 21% |
| | | | | | HOMO, HOMO → LUMO, LUMO 16% |
| S1 | 527.60 | 5,235 | 310.21 | $S_0 \to S_{17}$ | HOMO-3 → LUMO 11% |
| | | | | | HOMO-1 → LUMO+3 23% |
| | | | | | HOMO → LUMO+5 13% |
| | 422.00 | 48,129 | 4,457.65 | $S_0 \to S_{39}$ | HOMO-1 → LUMO+7 19% |
| S2 | 736.25 | 10,467 | 318.48 | $S_0 \to S_3$ | HOMO-1 → LUMO 27% |
| | | | | | HOMO → LUMO+2 20% |
| | | | | | HOMO, HOMO → LUMO, LUMO 11% |
| | 506.89 | 173,322 | 1,1126.7 | $S_0 \to S_{33}$ | HOMO-2 → LUMO+2 14% |
| T1 | 508.14 | 34,837 | 2,225.48 | $S_0 \to S_{40}$ | HOMO-1 → LUMO+3 18% |
| | | | | | HOMO-1 → LUMO+6 15% |
| | 439.04 | 171,462 | 14,672.23 | $S_0 \to S_{76}$ | HOMO, HOMO → LUMO, LUMO+1 16% |
| T2 | 611.97 | 47,457 | 2,090.15 | $S_0 \to S_{21}$ | HOMO-1 → LUMO+5 17% |
| | 511.91 | 473,809 | 29,822.97 | $S_0 \to S_{54}$ | HOMO-1, HOMO → LUMO, LUMO+1 12% |
| Q | 604.80 | 80,510 | 3,630.44 | $S_0 \to S_{19}$ | HOMO-5 → LUMO+1 13% |
| | | | | | HOMO-1 → LUMO+5 22% |
| | | | | | HOMO → LUMO+7 15% |
| | 506.89 | 512,695 | 32,913.3 | $S_0 \to S_{57}$ | HOMO-3 → LUMO+1 21% |

increased in a same extent. For molecules T1, T2, and Q, as the cyclic conjugation formed and the donor group introduced, $\delta_{max}$ in the longer-wavelength band shows about sevenfold larger than that of S1 and S2, but the enhancement of $\delta_{max}$ in shorter wavelength band is just about threefold. This is more beneficial to TPA application in practical for the more enlarged $\delta_{max}$ in the longer wavelength band. Insight into the relations between the $\delta$ values and molecular structures, we found that the $\delta$ values of the longer and shorter wavelength bands of studied molecules are all enlarged as the donor groups introduced into the backbone or formed the cyclic conjugation. Analyzing the impact
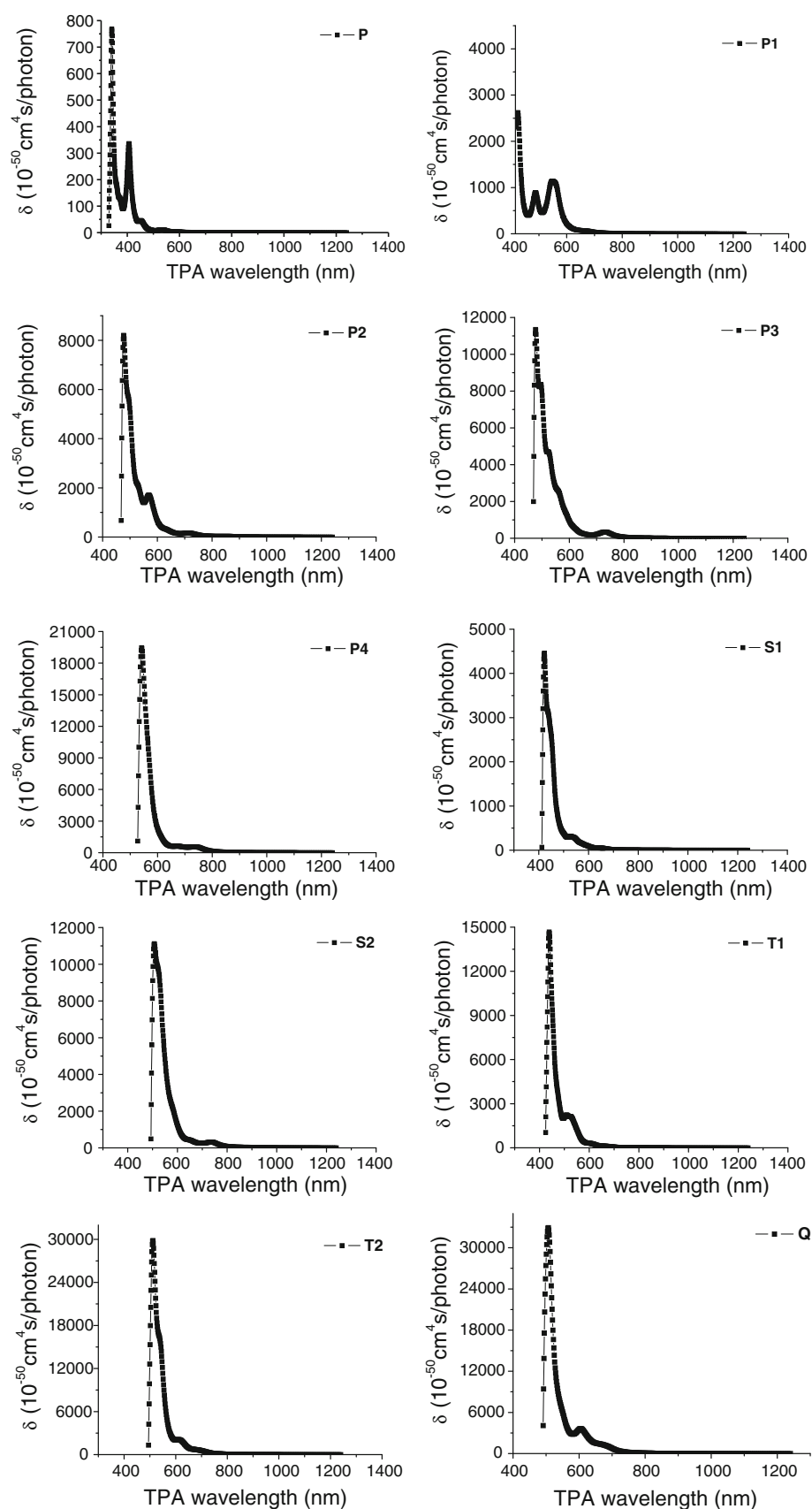
**Fig. 3** Two-photon absorption spectra

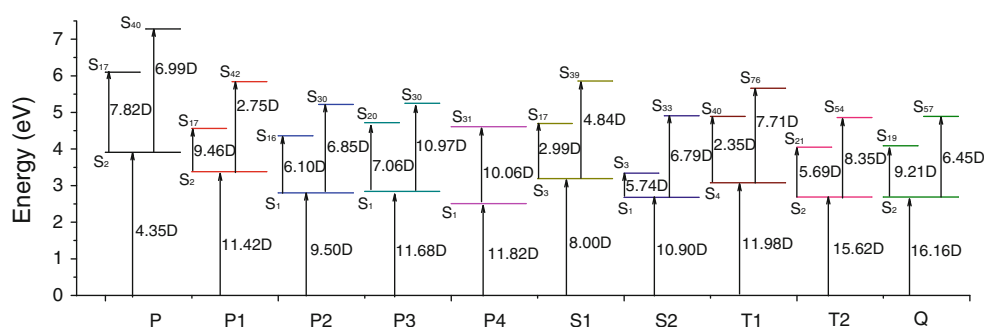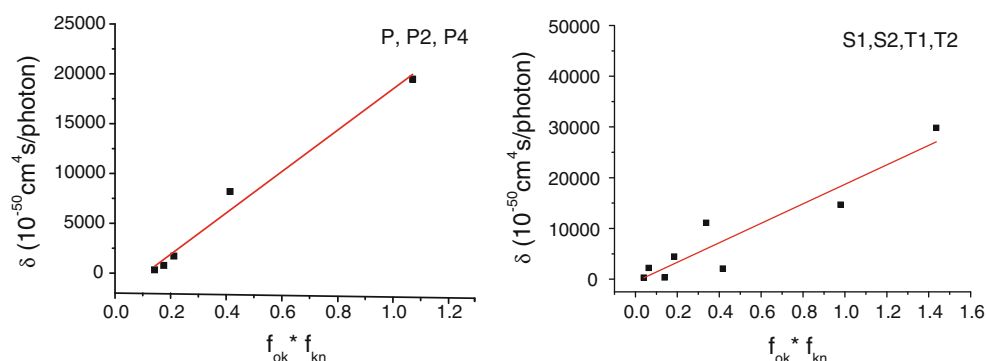**Fig. 4** Scheme of the calculated transition dipole moments and energy levels



**Fig. 5** Plot of $\delta_{max}$ vs. $f_{0k}*f_{kn}$



factors of $\delta_{max}$ according to three-state model [32, 36], the TPA cross-section is proportional to the square of $M_{0k}$ and $M_{kn}$ and it is inversely proportional to the square of the energy detuning term ($E_{0k} - E_{0n}/2$). So, when the donor groups are introduced into the molecules or formed the cyclic conjugation, the $M_{0k}$ and $M_{kn}$ values increase (Fig. 4), and lead to the $\delta$ values increase too. For molecules S1 and S2, the $\lambda^{(2)}$ values are largely red shifted compared with molecules P and P2, and the $\delta$ values corresponding to the shorter wavelength bands are greatly enhanced, while the $\delta$ values located in the longer wavelength bands are decreased as the new conjugation segments introduced. This can also be explained by the three-state model, and from which we deduce that the transitions correspond to shorter wavelength bands can effectively increase the intramolecular charge transfer (ICT) when new conjugation segments are introduced. Comparing the $\delta$ values of the dimers (T1 and T2) with their monomers (S1 and S2), we found that the $\delta$ values corresponding to the longer wavelength band are enlarged more than seven times, while the $\delta$ in shorter wavelength band just increases about three times. According to the calculated transition dipole moments (Fig. 4), the $M_{0k}$ and $M_{kn}$ values of T1 and T2 in short or long wavelength band are larger than their corresponding values of S1 and S2. So, it is obvious that the changing trend of TPA cross-sections can be explained by the three-state model too. Compared the $\delta$ values of the longer wavelength bands of T1 with that of T2, they do not change greatly, but only with a 7 time enhancement compared with the pyrene backbone. The $\delta_{max}$ value of the shorter wavelength band (511.91 nm) of

molecule T2 reaches 29,822.97 GM, about 40 times increases along with the $\lambda^{(2)}$ shifts from 341.18 to 511.91 nm.

The above results show that increasing the number of introduced donor group or forming a circular conjugated dimer can greatly increase the oscillator strength ($f$) of maximum OPA peak; meanwhile, the $\delta$ values are also effectively enlarged. So, we further studied the relations between them in the present study. Figure 5 shows the relationship between $\delta_{max}$ and the product of the $f_{0k}$ and $f_{kn}$ ($f_{0k}$: the $f$ between the ground state and intermediate state; $f_{kn}$: the $f$ between the intermediate state and final state in the TPA process; Concluding $\delta$ in the shorter and longer-wavelength bands). We can found that with the number of donor group increasing, the product of the $f_{0k}$ and $f_{kn}$ versus the $\delta_{max}$ of P, P2, and P4, presents a well linear relationship. For S1, T1, S2, and T2, the plots of $\delta_{max}$ versus the product of the $f_{0k}$ and $f_{kn}$ are averagely distributed along the fitted line. Thus, we can deduce that the $\delta$ and the product of $f_{0k}$ and $f_{kn}$ are proportional to each other, which suggested that $f$ is another important impact factor for $\delta_{max}$.

In order to further investigate how the molecular structures affect the frontier molecular orbital and confirm the internal factors which can affect TPA properties, we list the molecular orbitals related to main transitions in TPA process in Fig. 6. The electron densities of HOMO are distributed orderly of almost all the molecules and they are well-proportioned on the main body (pyrene) and the conjugated segments, while the electron densities of LUMO are all locate at pyrene main body. It is found that
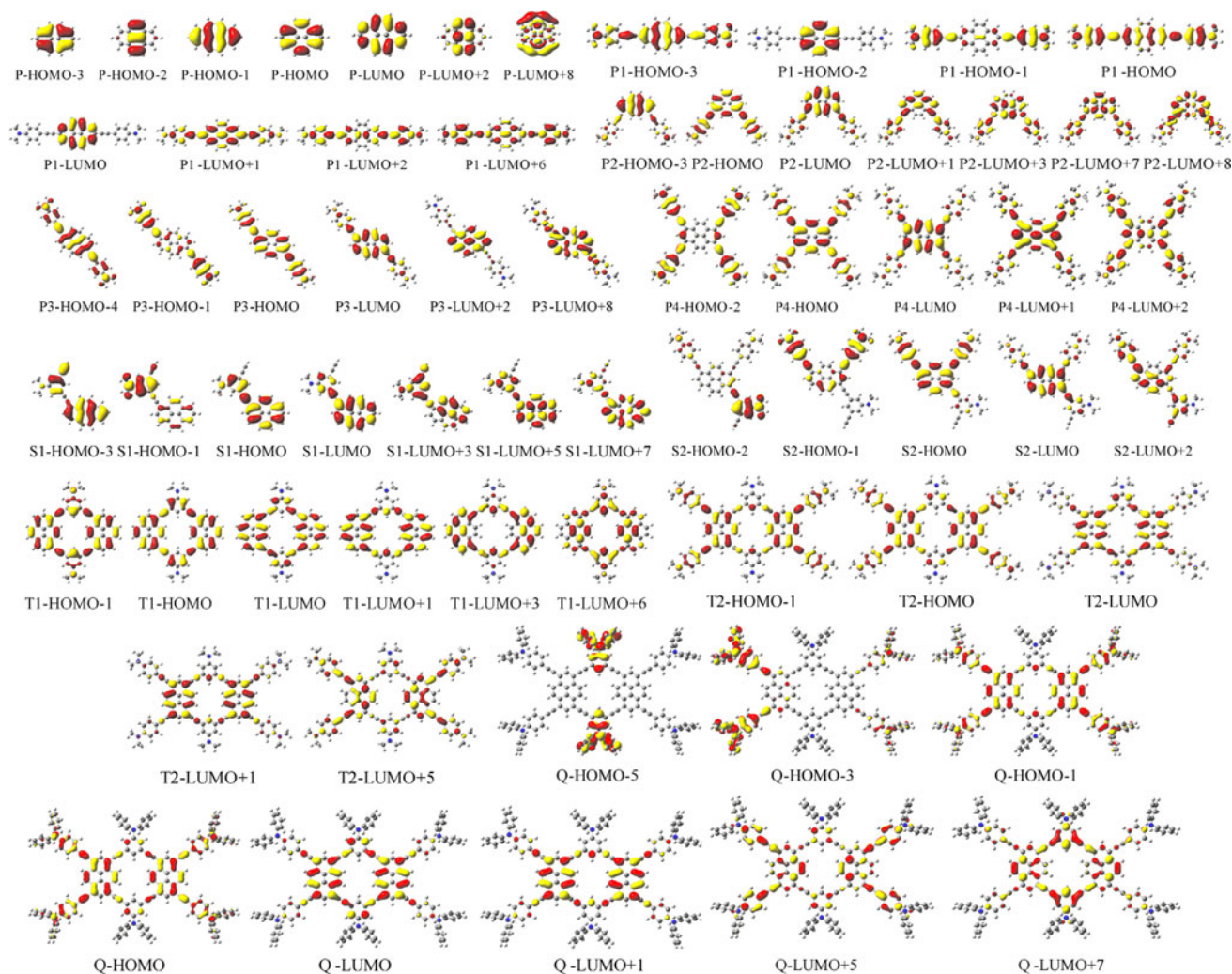
**Fig. 6** Contour surfaces of the frontier orbitals relevant to OPA and TPA for the studied molecules

the electron transfer occurred between the donor group and the main body during the TPA process, and the molecules exhibited large $\delta_{max}$ has high electron transfer efficiency, such as molecule P4. So, the $\delta_{max}$ of pyrene derivatives are enlarged by introducing donor groups and extending conjugation length. Observing the frontier orbitals of molecules T2 and Q, we can also find that replacing the methyl group with phenyl on the substituent R do not extend the distributions of electron density on occupied orbitals effectively, and the electron transfer related to phenyl group during the TPA process changes little. So the $\delta_{max}$ of molecule Q increases un-obviously compared with molecule T2.

# 4 Conclusion

The geometrical structure, OPA and TPA properties, and electronic structure of pyrene derivatives were studied theoretically. Calculated results show that almost all the pyrene derivatives exhibit two TPA peaks. Introducing the donor group to pyrene, increasing the number of donor group and extending the conjugated length make the maximum TPA position bathochromic shift and the $\Delta E_{H-L}$ decrease, and they are all efficient ways to enlarge the maximum TPA cross-section ($\delta_{max}$) of pyrene derivatives. Furthermore, changing the donor group position can also affect the $\delta_{max}$, that is, introducing donor groups on shoulder position and locating them at diagonal position, can lead pyrene molecules exhibit large $\delta_{max}$. Insight into the circular conjugated pyrene molecule, it is an effective way to increase the $\delta_{max}$ by forming the circular conjugated system, but when introducing donor group to the circular system the increasing trend will be diminished. This can be illustrated by the molecular orbital analysis. Furthermore, the $\delta_{max}$ is proportional to the product of $f_{0k}$ and $f_{kn}$, which can be enhanced as the number of conjugated donor group increased or a circular conjugated dimer formed. Taken

together, the present work theoretically studied the OPA and TPA properties of pyrene derivatives, which give us some basic principles to design pyrene derivatives with large TPA cross-sections. This shed light into the significance of the pyrene derivatives as promising fluorescent probes in biochemistry when it was linked to some special recognizing groups.

# References

1. Göppert-Mayer M (1931) Ann Phys 401:273–294
2. Dvornikov AS, Rentzepis PM (1995) Opt Commun 119:341–346
3. Cumpston BH, Ananthavel SP, Barlow S, Dyer DL, Ehrlich JE, Erskine LL, Heikal AA, Kuebler SM, Lee IYS, Maughon MD, Qin J, Rockel H, Rumi M, Wu X-L, Marder SR, Perry JW (1999) Nature 398:51–54
4. Denk W, Svoboda K (1997) Neuron 18:351–357
5. Allain C, Schmidt F, Lartia R, Bordeau G, Fiorini-Debuisschert C, Charra F, Tauc P, Teulade-Fichou M-P (2007) Chem Bio Chem 8:424–433
6. Fleitz PA, Brant MC, Sutherland RL, Strohkendl FP, Larsen RJ, Dalton LR (1998) Proc SPIE 3472:91–97
7. Ehrlich JE, Wu XL, Lee LY, Hu ZY, Rockel H, Marder SR, Perry JW (1997) Opt Lett 22:1843–1845
8. Denk W, Strickler JH, Webb WW (1990) Science 248:73–76
9. Ikeda C, Yoon ZS, Park M, Inoue H, Kim D, Osuka A (2005) J Am Chem Soc 127:534–535
10. Zhao Y, Ren AM, Feng JK, Sun CC (2008) J Chem Phys 109:014301-1–014301-10
11. Lucas LA, Delongchamp DM, Richter LJ, Kline RJ, Fischer DA, Kaafarani BR, Jabbour GE (2008) Chem Mater 20:5743–5749
12. de Halleux V, Calbert JP, Brocorens P, Cornil J, Declercq JP, JL Brédas, Y Geerts (2004) Adv Funct Mater 14:649–659
13. Daub J, Engl R, Kurzawa J, Miller SE, Schneider S, Stockmann A, Wasielewski MR (2001) J Phys Chem A 105:5655–5665
14. Jones G, Vullev VI (2002) Org Lett 4:4001–4004
15. Caruso F, Donath E, Möhwald H, Georgieva R (1998) Macromolecules 31:7365–7377
16. Tong G, Lawlor JM, Tregear GW, Haralambidis J (1995) J Am Chem Soc 117:12151–12158
17. Lewis FD, Zhang YF, Letsinger RL (1997) J Am Chem Soc 119:5451–5452
18. Kim SK, Kim SH, Kim HJ, Lee SH, Lee SW, Ko J, Bartsch RA, Kim JS (2005) Inorg Chem 44:7866–7875
19. Conlon P, Yang CJ, Wu Y, Chen Y, Martinez K, Kim Y, Stevens N, Marti AA, Jockusch S, Turro NJ, Tan W (2008) J Am Chem Soc 130:336–342
20. Paris PL, Langenhan JM, Kool ET (1998) Nucleic Acids Res 26:3789–3793
21. Masuko M, Ohtani H, Ebata K, Akira Shimadzu (1998) Nucleic Acids Res 26:5409–5416
22. Fujimoto K, Shimizu H, Inouye M (2004) J Org Chem 69:3271–3275
23. Valis L, Amann N, Wagenknecht H (2005) Org Biomol Chem 3:36–38
24. Hwang GT, Seo YJ, Kim BH (2004) J Am Chem Soc 126:6528–6529
25. Wagner C, Rist M, Mayer-Enthart E, Wagenknecht H (2005) Org Biomol Chem 3:2062–2063
26. Yamana K, Fukunaga Y, Ohtani Y, Sato S, Nakamura M, Kim WJ, Akaikeb T, Maruyama A (2005) Chem Commun 2509–2511
27. Kim HM, Lee YO, Lim CS, Kim JS, Cho BR (2008) J Org Chem 73:5127–5130
28. Cha M, Torruellas WE, Stegeman GI, Horsthuis WHG, Möhlmann GR, Meth J (1994) Appl Phys Lett 65:2648–2650
29. Kogej T, Beljonne D, Meyers F, Perry JW, Marderm SR, Brédas JL (1998) Chem Phys Lett 298:1–3
30. Orr BJ, Ward JF (1971) Mol Phys 20:513–526
31. Bishop DM, Luis JM, Kirtman B (2002) J Chem Phys 116:9729–9739
32. Beljonne D, Wenseleers W, Zojer E, Shuai Z, Vogel H, Pond SJK, Perry JW, Marder SR, Brédas JL (2002) Adv Funct Mater 2:631–641
33. Becke AD (1993) J Chem Phys 98:1372–1377
34. Francl MM, Pietro WJ, Hehre WJ, Binkley JS, Gordon MS, Defrees DJ, Pople JA (1982) J Chem Phys 77:3654–3665
35. Ridley J, Zerner MC (1973) Theo Chim Acta 32:111–134
36. Albota M, Beljonne D, Brédas JL, Ehrlich JE, Fu JY, Heikal AA, Hess SE, Kogej T, Levin MD, Marder SR, McCord-Maughon D, Perry JW, Röckel H, Rumi M, Subramaniam G, Webb WW, Wu XL, Xu C (1998) Science 281:1653–1656
37. Òscar RP, Luo Y, Ågren H (2006) J Chem Phys 124:094310-1–094310-5
38. Ma WB, Wu YQ, Gu DH, Gan FX (2006) J Mol Struct Theochem 772:81–87
39. Frisch MJ, Trucks GW, Schlegel HB, Scuseria GE, Robb MA, Cheeseman JR, Montgomery JA, Vreven TJ, Kudin KN, Burant JC, Millam JM, Yengar SS, Tomasi J, Barone V, Mennucci B, Cossi M, Scalmani G, Rega N, Petersson GA, Nakatsuji H, Hada M, Ehara M, Toyota K, Fukuda R, Hasegawa J, Ishida M, Nakajima T, Honda Y, Kitao O, Nakai H, Klene M, Li X, Knox JE, Hratchian HP, Cross JB, Adamo C, Jaramillo J, Gomperts R, Startmann RE, Yazyev O, Austin AJ, Cammi R, Pomelli C, Ochterski JW, Ayala PY, Morokuma K, Voth GA, Salvador P, Dannenberg JJ, Zakrzewski VG, Dapprich JM, Daniels AD, Strain MC, Farkas O, Malick DK, Rabuck AD, Raghavachari K, Foresman JB, Ortiz JV, Cui Q, Baboul AG, Cliffors S, Cioslowski J, Stefanov BB, Liu G, Liashenko A, Piskorz I, Komaromi I, Martin RL, Fox DJ, Keith T, Al-Laham MA, Peng CY, Manayakkara A, Challacombe M, Gill PMW, Johnson BG, Chen W, Wong MW, Gonzalez C, Pople JA (2003) Gaussian revision C. 02. Gaussian, Inc., Pittsburgh, PA